Heterogeneous nucleation of solid Al from the melt by Al_3Ti: molecular dynamic simulations

Junsheng Wang[1], Andrew Horsfield[1], Peter D. Lee[1], and Peter Brommer[2]
[1]Department of Materials, Imperial College, London SW7 2AZ, UK
[2]Institut für Theoretische und Angewandte Physik, Universität Stuttgart, 70550 Stuttgart, Germany

ABSTRACT

It has been known experimentally for some time that Al_3Ti is a powerful nucleant for the solidification of aluminum from the melt; however, a full microscopic understanding is still lacking. To develop this understanding we have performed molecular dynamics simulations of the nucleation and early stages of growth using published embedded atom method (EAM) potentials for Al-Ti, but modified by us to stabilize the $D0_{22}$ structure. We discover that Al_3Ti can indeed be very effective in promoting the growth of solid Al, but the manner in which growth takes place depends sensitively on the surface on which the Al nucleates. In particular, complete growth of solid Al from the liquid on the (001) and (110) surfaces of Al_3Ti occurs at a lower temperature than on the (112) surface. This anisotropy agrees with observations in previous experiments [Greer, et al., Acta Mater. 48, 2823 (2000)]. We explain this observation in terms of interfacial energies. On the (111) surface of Al the solid-liquid interfacial energy is highest, while the solid-vacuum energy is lowest. Our simulations also show that the extent of ordering taking place in liquid Al close to the Al_3Ti substrate above the melting point correlates well with the effectiveness of the substrate as a nucleant below the melting temperature: this could provide a computationally efficient scheme to identify good nucleants.

Keyword: Heterogeneous Nucleation; Molecular Dynamics; Solidification; Grain Refinement; Kinetics; Al_3Ti; Aluminum.

I. INTRODUCTION

For over 80 years [1] the addition of titanium has been known to cause grain refinement in aluminum alloys. However, the mechanism by which titanium acts is still a subject of strong dispute, with the current theories (incorporating the influence of boron as well) being divided into six different groupings in a recent review[2]. Several of these theories are based on the heterogeneous nucleation of α-Al on an Al_3Ti particle, with conflicting suggestions whether it is the morphology[3], size[2], or crystallographic face of the Al_3Ti particle[4] that is the most important consideration.

Recent experimental studies by Schumacher, Greer, et al[5] have indicated that α-Al nucleates best on the (112) face of the Al_3Ti particle. This face is metastable, and not found in equilibrium particles of Al_3Ti in molten Al. Schumacher and Greer [6] added TiB_2 particles (with and without excess Ti) into a molten $Al_{85}Ni_5Y_8Co_2$ glass, and then quenched in the early stages of Al_3Ti and α-Al formation by using ribbon casting to achieve a cooling rate of ~10^6 Ks^{-1}. Using transmission electron microscopy (TEM) they found that some α-Al had nucleated on the (0001) face of the TiB_2 particles, but not on the other faces. With 0.1at% excess Ti added, an Al_3Ti layer forms on the TiB_2 particles, thickening with longer holds before quenching. The primary orientation relationship found between the particles was $(0001)_{TiB2}//(112)_{Al3Ti}//(111)_{\alpha\text{-}Al}$. Interestingly in their studies they found the Al_3Ti formed on the TiB_2 with the meta-stable (112) face exposed. Their studies suggest that even the heterogeneous nuclei of TiB_2 act via the formation of Al_3Ti layers prior to the nucleation of α-Al. Identifying the exact crystal orientation relationships between the different phases has been a subject of ongoing TEM[7] experiments and more recently Inqbal *et al.* [8-10] have performed x-ray diffraction investigations. Inqbal *et al.* performed *in situ* x-ray diffraction experiments on pure Al with different volume fractions of TiB_2 inoculants and Ti solute concentrations using a synchrotron X-ray source. They identified the presence of a metastable Al_3Ti phase prior to solidification in the Al melt.

Although Al_3Ti has been shown repeatedly by experiment to dramatically decrease the critical undercooling for α-Al nucleation, the mechanism by which α-Al nucleates on top of Al_3Ti is still not clear. There are a number of hypotheses based on the analysis of final microstructures [2, 11, 12] and crystal orientation

relationships (ORs) [13, 14]. However, an atomistic understanding is still lacking. In this paper, we present the first detailed atomistic investigation of α-Al nucleation on top of an Al_3Ti substrate.

Nucleation is a kinetic process occurring at the atomic scale. Molecular Dynamics (MD) allows us to follow fast atomic kinetic processes directly. Using *embedded atom method* (EAM) [15, 16] potentials for the Al-Ti system, we performed classical MD simulations to observe directly the initial stages of solidification in Al melts. We investigate the effect on nucleation of different surfaces in order to explain the orientation relationship [7] between Al_3Ti and α-Al observed in experiments. To explain the negligible undercoolings or "*free growth*" in experiments[17], we characterize the structural ordering close to the Al_3Ti substrate as a function of superheating in the Al melt using a previously proposed disorder parameter[18] and other quantitative measures of the ordering at the solid/liquid interface. We thus add a true microscopic understanding to the knowledge already derived from experimental observations.

II. METHODOLOGY

A. EAM Potential

The EAM was initially proposed by Daw and Baskes [15, 19]. It describes the total energy of a system as a combination of two separate parts: a pair interaction term ($\Phi(r_{ij})$) dependant only on interatomic distance (r_{ij}) and an EAM functional ($F(\rho)$) which is a function of average electron density ($\overline{\rho}$):

$$E_{tot} = \frac{1}{2}\sum_{\substack{i,j \\ i \neq j}} \Phi_{ij}(r_{ij}) + \sum_i F_i(\overline{\rho}_i) \tag{1}$$

with

$$\overline{\rho}_i = \sum_{j(i \neq j)} \rho_j(r_{ij}) \tag{2}$$

where $\rho_t(r)$ is the atomic electron density at r from the atom at site i. There are different forms of EAM potentials depending on how the two-body and many body terms are calculated [20]. For example, the Finnis-Sinclair [21] potential is derived from the second moment approximation to tight binding theory, and has been successful for simulating the properties of transition metals. Because the many body interactions can be

defined in terms of the local electronic density, EAM potentials can also find their physical root in density functional theory (DFT) [20]. The EAM potential form can also be taken to be completely empirical, in which case they are then sometimes called glue potentials[22]. MD codes employing this kind of semi-empirical potential for calculating forces and solving Newton's equation of motion for calculating velocities are extremely useful for fast simulations of transition phenomena in large systems.

For the Al-Ti alloying system, there are two EAM potentials available and both of them are developed from fits to experimental and *ab initio* calculation data [23, 24]. However, neither of them predicts the correct order for the most stable Al_3Ti structures ($D0_{22}$ is more stable than $L1_2$) because the energy difference between those two structures is only 0.02 eV/atom[25]. Farkas [23] predicted the $L1_2$ structure to be 0.03 eV lower in energy than the $D0_{22}$ structure and the potential developed by Zope and Mishin [24] gives the same order but a smaller value for the difference (0.01 eV/atom). The $D0_{22}$ structure is tetragonal (the ratio c/a differs from 2) and formed from two fcc-like unit cells stacked along the c direction, while the $L1_2$ structure is simply fcc-like. Farkas [23] found the addition of angular terms to the potential did not help to predict the correct order and proposed that the stability of the two phases is controlled mainly by the pair term. Below we describe the small change we make to the Al-Ti pair term of the potential of Zope and Mishin [24] to obtain the correct structural ordering.

B. Molecular Dynamics Simulations

Two molecular dynamic parallel simulation packages (DL_POLY [26, 27] and LAMMPS[28, 29]) were used. For both, to solve Newton's equation of motion we used the velocity-Verlet integration algorithm [30]. Using our modified Zope and Mishin EAM potential, we investigated the dynamics of Al liquid in contact with solid Al_3Ti. Because the atomic interactions between Al-Al, Ti-Ti, and Ti-Al are taken into account naturally by the EAM potential no matter whether they are in the bulk solid (S) or liquid (L), or at the S/L interface, there is no need to fix atoms in the solid in order to observe the ordering at the interface, unlike previous studies [18]. However, the maximum superheating is limited by the melting temperature of the Al_3Ti structure.

To begin the simulations of liquid Al on top of Al_3Ti substrates, perfect $D0_{22}$ crystalline Al_3Ti was created together with fcc Al for three different interfaces: Al(110)//Al_3Ti(110), Al(001)//Al_3Ti(001),and

Al(111)//Al_3Ti(112); the relative orientations in the plane of the interface is not important at this stage as the Al is melted and the final orientation will be determined by the nucleation step. For static calculation, the exact matching orientations for edges along x- and y-axis are listed in Table 1. The lattice parameters were $a = b = 3.8537$ Å, $c = 8.58390$ Å for Al_3Ti [31], with ideal inter-plane spacing (d-spacing) increasing from (110) to (001), with almost twice the (110) d-spacing along the (112) direction. The details for the supercells containing liquid Al in contact with solid Al_3Ti for three types of interface are given in Table 1. There were 2048 liquid Al atoms and 768 Al_3Ti units for the (001) interface, and 3456 liquid Al atoms and 864 Al_3Ti units for the other two. We believe the Al_3Ti region represents well its bulk properties because our slab calculations of Al_3Ti surface energy (see below) produce consistent values when the number of planes is larger than ten. The liquid Al is thick enough to allow us to see the range of ordering from solid-like to liquid. Therefore the simulation geometry is large enough that we can extract quantitative information for the three different interfaces, while being small enough to allow a large number of simulations to be performed as described below.

Table 1 Simulation supercell geometry

System	Al_3Ti d-spacing (Å)	Number of planes in Al_3Ti	Number of Al_3Ti units	Number of liquid Al atoms
Al(110)//Al_3Ti(110)	1.36	$24_{[\bar{1}10]} \times 24_{[001]} \times 24_{[110]}$	864 (6×6×12)	3456
Al(001)//Al_3Ti(001)	2.15	$16_{[100]} \times 16_{[010]} \times 24_{[001]}$	768 (8×8×6)	2048
Al(111)//Al_3Ti(112)	2.34	$24_{[\bar{1}10]} \times 32_{[11\bar{2}]} \times 18_{[112]}$	864 (8×8×6)	3456

As we shall see, the melting point of Al for our potential is about 870K. Two kinds of molecular dynamic simulations were performed: 1. tests above the melting point (T > 870 K); and 2. nucleation runs just below it (T < 870 K). As shown in Table 2, both kinds of simulation used an NPT ensemble [32] with zero pressure. Above 870 K we performed 7 runs for each system with temperatures ranging from 875 to 1025 K in steps of 25 K; for undercooled systems we ran 21 tests for each system with temperatures ranging from 850 to 870 K in steps of 1 K: see Table 2. We also repeated the nucleation runs using an NVT ensemble with the

cell size in the plane of the interface adjusted to the substrate lattice parameter for the given temperature. Our conclusions were the same in this case.

Table 2 Simulation conditions

System	Number of atoms	Pressure	Molten			Undercooled		
			T_{max}(K)	T_{min}(K)	ΔT(K)	T_{max}(K)	T_{min}(K)	ΔT(K)
Al(110)//Al_3Ti(110)	6912	0	1025	875	25	870	850	1
Al(001)//Al_3Ti(001)	5120	0	1025	875	25	870	850	1
Al(110)//Al_3Ti(112)	6912	0	1025	875	25	870	850	1

To set up the run for each system, the Al was melted at 1273 K and an average pressure of 0 Pa using the Hoover NVT ensemble [32] implemented in DL_POLY [26, 27]. The liquid Al atoms were then combined with Al_3Ti solid for the three orientations of the terminating planes of Al_3Ti ((111), (100), and (110)), and then equilibrated in LAMMPS instead of DL_POLY. We use LAMMPS because its NPT ensemble implementation allows us to establish zero pressure in both axial and off-axial directions while maintaining a vacuum region on top of the liquid. After equilibrating for 1 ps at constant volume, the MD simulations were carried out at constant pressure (0 Pa) and temperature. Periodic boundary conditions were applied in the *x*- and *y*-directions. In the *z*-direction, two S/L interfaces interact with each other if periodic boundary conditions are applied, leading to spurious effects. This is because the stress created at the S/L interface cannot be effectively released in the periodic cell, introducing arbitrary shearing in the Al_3Ti structure. It has been observed that this shearing is enough to create dislocations. In reality, no stress is accommodated at the S/L interface during solidification because it is effectively released at the free liquid surfaces. Thus we always include vacuum above the liquid in our simulations. To simulate nucleation and growth the supercells were finally cooled down to various degrees of undercooling using LAMMPS. In order to observe the nucleation at smaller undercoolings, the MD calculations were run for 1200ps.

C. Analysis of Density Profile

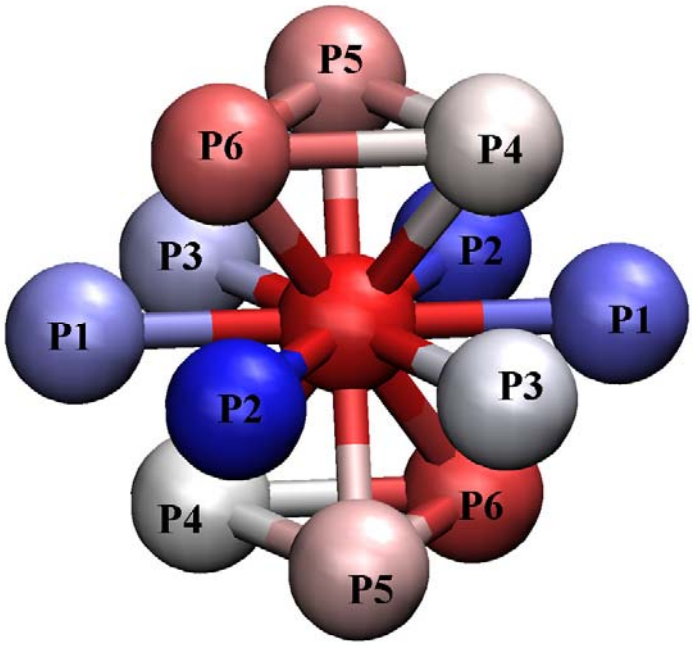

Fig. 1 Illustration of opposite pairs of atoms in the fcc structure.

To characterize the atomic distribution across the solid/liquid (S/L) interface, the density profile ($\rho(z)$) was calculated using the following formula [18, 33]:

$$\rho(z) = \frac{\langle N_z \rangle}{A_{xy}\Delta z} \tag{3}$$

where $<N_z>$ is the time averaged number of atoms in a bin of width Δz and A_{xy} is the area of the S/L interface region. The resulting profile is very sensitive to the choice of bin size (Δz). To obtain a good spatial density distribution, the density fluctuations inside a bin have to be much smaller than the average variation of density over the distance defined by the bin size. For the calculation of density profiles above the melting point we found using 400 bins was optimal; the time averages were taken over 100 snapshots separated by 0.1ps.

D. Quantification of Structural Ordering

Because nucleation involves a transition from disordered liquid to ordered solid, a measure of the local ordering at the S/L interface is a very informative tool for interpreting the evolution of the interface. Many

authors have proposed methods to characterize the short ranged structural ordering during solidification including the Common Neighbor Analysis (CNA) [34], the Centrosymmetry Parameter (CSP) [35], the Common Neighborhood Parameter (CNP) [36], and the Ordering Discriminator Function (ODF) [37]. We use the CSP, a measure of the deviation from centrosymmetry in a given centrosymmetric structure such as fcc, as it is easier to interpret than the others. Not only can liquid and solid be effectively distinguished using this parameter but also defect sites in the Al_3Ti substrate. For an fcc structure the CSP is defined as [35]:

$$\alpha = \sum_{i=1,6} \left| R_i + R_{i+6} \right|^2 \tag{4}$$

where R_i and R_{i+6} are bond vectors corresponding to the six pairs of opposite nearest neighbors, where the nearest neighbors are identified by finding the opposite atoms closest to the positions defined by the undistorted nearest neighbor vectors (see Fig.1). For bulk Al in the fcc structure, $\alpha = 0$, for the (001) surface $\alpha = 24.9$ Å^2, for an intrinsic stacking fault $\alpha = 8.3$ Å^2, for atoms midway between fcc and hcp $\alpha = 2.1$ Å^2, and for liquid atoms with disordered structure $8.3 < \alpha < 24.9$ Å^2 [36].

Buta *et al* [33] proposed a quantity that can measure both long and short ranged order, namely the two dimensional (2D) structure factor $S_{2D}(k)$ that characterizes the lateral structural ordering [38]:

$$S_{2D}(k) = \frac{1}{N} \sum_{i,j}^{N} \left\langle \exp\left[i\vec{k} \cdot (\vec{r}_i - \vec{r}_j) \right] \right\rangle = \frac{1}{N} \sum_{i,j}^{N} \cos\left[k_x (x_i - x_j) + k_y (y_i - y_j) \right] \tag{5}$$

Atoms in each plane parallel to the S/L interface are projected onto the original *xy* plane, so only the *x* and *y* coordinates appear in the computations for this quantity. This two-dimensional Fourier transformation of the density fluctuations gives a periodic pattern similar to x-ray or neutron scattering experiments, and is particularly useful tool for understanding the lateral ordering on the $Al_3Ti(112)$ surface at the beginning of continuous growth.

III. RESULTS AND DISCUSSIONS

A. EAM Potential

Since the EAM potential developed by Zope and Mishin (Z&M) [24] gives very good property predictions at high temperature, we started with this potential. To stabilize the $D0_{22}$ structure we slightly modified the cross

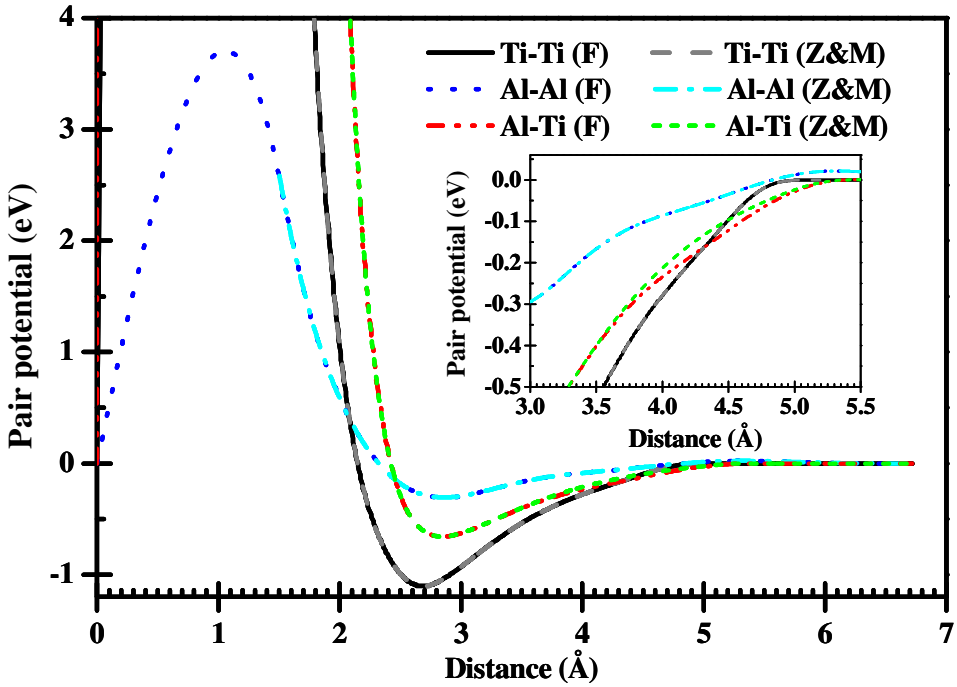

Fig. 2 Comparison of fitted pair potentials (F) and those published by Zope and Mishin (Z&M) [24].

Al-Ti pair potential with the force matching method[39], i.e. by fitting to a large database of *ab initio* molecular dynamics data calculated using the Vienna Ab-initio Simulation Package (VASP)[40-43]. We used Projector Augmented Waves[44, 45] to manage the rapidly varying components of the wavefunctions in the vicinity of the nuclei, and the PW91[46, 47] gradient corrected density functional to describe electron exchange and correlation. In total, 25 sets of data were calculated using *ab initio* MD at different temperatures ranging from 0 to 1300 K. Each dataset consisted of 144 atomic configurations, for which we computed the forces, energy, and stress terms. Using *potfit* [48], to fit our new potential, the fitting process was automated, but we only allowed the cross Al-Ti pair potentials to be modified, as shown in Fig. 1.

In particular, in order to keep the excellent capability for predicting materials properties which Zope and Mishin have shown previously [24], we fixed all the other parts (including electron densities and EAM functions) and kept the same cutoff as their potentials during the fittings. The fitted (indicated by F in Fig. 2) Al-Ti potential only deviates from the original (indicated by Z&M in Fig. 2) at a distance corresponding to the second neighbors of atoms in the $D0_{22}$ structure. Using this new EAM potential the properties of fcc Al and hcp Ti were calculated and compared to the results from the Z&M potential, and exact agreement was found. For Ti_3Al intermetallics (see Table 3) the new potential predicts a lattice parameter that is 0.5% larger

than the experimental value, but gives a better prediction of *c/a* ratio [25, 49] which is important for the stability of the intermetallic structure, as pointed out by Farkas [23].

Table 3 Equilibrium properties of Ti_3Al predicted by the present EAM potential.

Property	Al_3Ti		Ti_3Al		
	Expt.	Present	Expt.	Z&M	Present
a_0 (Å)	3.854	3.923	5.77	5.784	5.8024
c/a	2.227	2.228	0.8007	0.821	0.8023
E_0 (*eV*/atom)	4.06	4.029	4.78	4.766	4.759

To investigate the relative stabilities of Al-Ti intermetallic compounds in different crystal structures, we calculated the formation energy for Al_3Ti, AlTi, and Ti_3Al, as shown in Table 4. In all calculations we used the same cutoff as in previous work for intermetallic compounds (r_{cutoff} = 5.75 Å) [24]. Both experimental and DFT results are also included with the energies given by Z&M EAM potential [24]. Although the present potential does not predict the exact values obtained from experiment, the agreement is usually reasonable, and, importantly for this work, for Al_3Ti it makes the $D0_{22}$ structure most stable instead of the $L1_2$ structure given by Z&M EAM potential [24]. For Ti_3Al the results are less good, with the $D0_{19}$ structure having a significantly lower energy than the $D0_{22}$ and $L1_2$ structures. However, in this work we always consider Al rich systems, so do not expect significant errors to arise from this.

Table 4 Comparison of formation energies, ΔH (eV/atom), of different compounds in the Al-Ti system.

Structure	Al_3Ti			AlTi			Ti_3Al		
	DFT	Z&M	Present	Expt.	Z&M	Present	Expt./DFT	Z&M	Present
$L1_0$	–	–	–	-(0.37~0.39)	-0.404	-0.4464	–	–	–
$L1_2$	–	-0.30	-0.2152	–	–	–	-0.28	-0.288	-0.1300
$D0_{22}$	-0.41	-0.29	-0.2962	–	–	–	-0.27, -0.25	-0.28	-0.2626
$D0_{19}$	–	-0.29	-0.2950	–	–	–	-0.25, -0.26	-0.289	-0.2978

The predicted energies of the Al (110), (001) and (111) surfaces were 0.81, 0.61, and 0.60 J/m^2, respectively, as shown in Table 5. These values compare well with previous calculations (0.79, 0.61, 0.60 J/m^2) using the Zope and Mishin potentials [24]: the origin of the small difference for the Al(110) surface energy is unclear.

The more close packed surfaces have the lower energy because their atomic environments are least disrupted by the severing of bonds. These predictions also match the range of values reported from experiments (from 0.60 [50] to 1.14 J/m^2 [51]) based on an assumption of isotropic surface energies. As shown in Table 5, the interfacial energies between Al and Al_3Ti also show strong anisotropy. The Al(111)//Al_3Ti(112) interface has the lowest energy among the three experimentally reported parallel interfaces [6]. This is because of the close match of lattice parameters, and indicates that heterogeneous nucleation may be preferred on the Al_3Ti(112) surface. We note that a crystal of Al_3Ti without a substrate will not have (112) planes as free surfaces[5], thus this surface must therefore be stabilized by the TiB_2 substrate it grows on.

Table 5 Ideal surface and interface formation energies for Al and Al_3Ti calculated using the current potential at 0K. Our computed melting temperatures for the different Al crystal orientations are also given.

Systems	(110)			(001)			(111)		
	Al	Al_3Ti	Al//Al_3Ti	Al	Al_3T	Al//Al_3Ti	Al	Al_3Ti	Al//Al_3Ti
Orientation	–	–	$[110]_{Al}//[110]_{Al\ 3Ti}$ $[001]_{Al}//[001]_{Al3Ti}$	–	–	$[100]_{Al}//[100]_{Al3Ti}$ $[010]_{Al}//[010]_{Al3Ti}$	–	–	$[110]_{Al}//[110]_{Al3Ti}$ $[111]_{Al}//[112]_{Al3Ti}$
Energy (J/m^2)	0.81	1.16	1.97	0.61	1.44	2.05	0.60	0.92	1.52
Melting Point (K)	871±3	–	–	–	–	–	870±4	1260±7	–

The experimental values of melting temperatures for Al and Al_3Ti are 933K [52] and 1685K [53], respectively. Because of anharmonic effects at high temperatures, it is difficult to fit the melting temperature correctly [24] while keeping a reasonable description of the mechanical properties of the solid state, especially for alloys. For our simulations we clearly need to know the melting temperature predicted by the potential as this tells us when we expect the liquid Al to solidify.

We determine the melting point as a function of crystal interface orientation using the S/L coexistence method previously developed by Morris *et al* [54]. Following Morris and Song [55], we prepared the melt above the melting temperature (T = 1273 K) and produced the hot solid at a temperature just below the melting point (T = 850 K). The two components were then combined to produce a semi-solid structure and equilibrated at the experimentally measured melting point (T = 933 K) using the NPT ensemble. After 10 ps

the fluctuation of temperature had reduced to ±5 K and the total volume was constant. An NVE simulation was then performed to allow the phase transformation. Because of the conversion from kinetic energy to potential energy the system temperature reduces and the pressure may also change, depending on whether the NPT equilibrated volume matches the coexistent one or not. As the initial guess for the melting temperature (the experimental value) may not be close to the melting point from the EAM potential, the pressure is normally not zero. This was resolved by repeating the NPT equilibration simulations with a reduced temperature until zero pressure was obtained in our final NVE runs. We found from the current EAM potential that the coexistence temperatures of pure Al are 871±3K and 870±4 K for (110) and (111) interfaces, respectively, showing that this is independent of crystal orientation. Finally we note that the melting temperature of Al_3Ti was measured to be 1260±7K for the (111) interface, thus will remain solid for all our simulations.

B. Heterogeneous Nucleation

In order to understand the first steps of the phase transformation from liquid to solid, we reduced the temperature from 870K to 850K in steps of 1K. At each temperature, the mixture of liquid Al and solid Al_3Ti was equilibrated for 1.2 ns using the NPT ensemble [32]. Interestingly, the nucleation temperature is found to be strongly anisotropic. At 860K a solid-like region always propagates through the liquid, but stops growing with liquid remaining when on top of the Al_3Ti(110) and (001) surfaces. The ordering stops about 10 layers into the liquid on the Al_3Ti(110) surface, as can be seen by comparing Fig. 3a to Fig. 3c. The thickness of solid for the (001) surface is approximately the same. However, continuous growth of the solid phase out to the vacuum occurs on the Al_3Ti(112) surface, as can be observed by comparing Fig. 3b to Fig. 3d. We therefore conclude that solid Al grows on the Al_3Ti(112) surface when the undercooling is small, but growth is inhibited for the other surfaces. In passing we note that the Al grows on the substrates with the following orientations in the plane of the interface : [110]Al//[110]Al_3Ti, and [111]Al//[112]Al_3Ti.

When we reduce the temperature further, the liquid on Al_3Ti(110) becomes fully solid at 852K, and that on the Al_3Ti(001) surface solidifies below 858K. The nucleation temperature on the Al_3Ti(112) surface was found to be 862K. Unlike homogeneous nucleation studies [56], the nucleation time is not measured explicitly

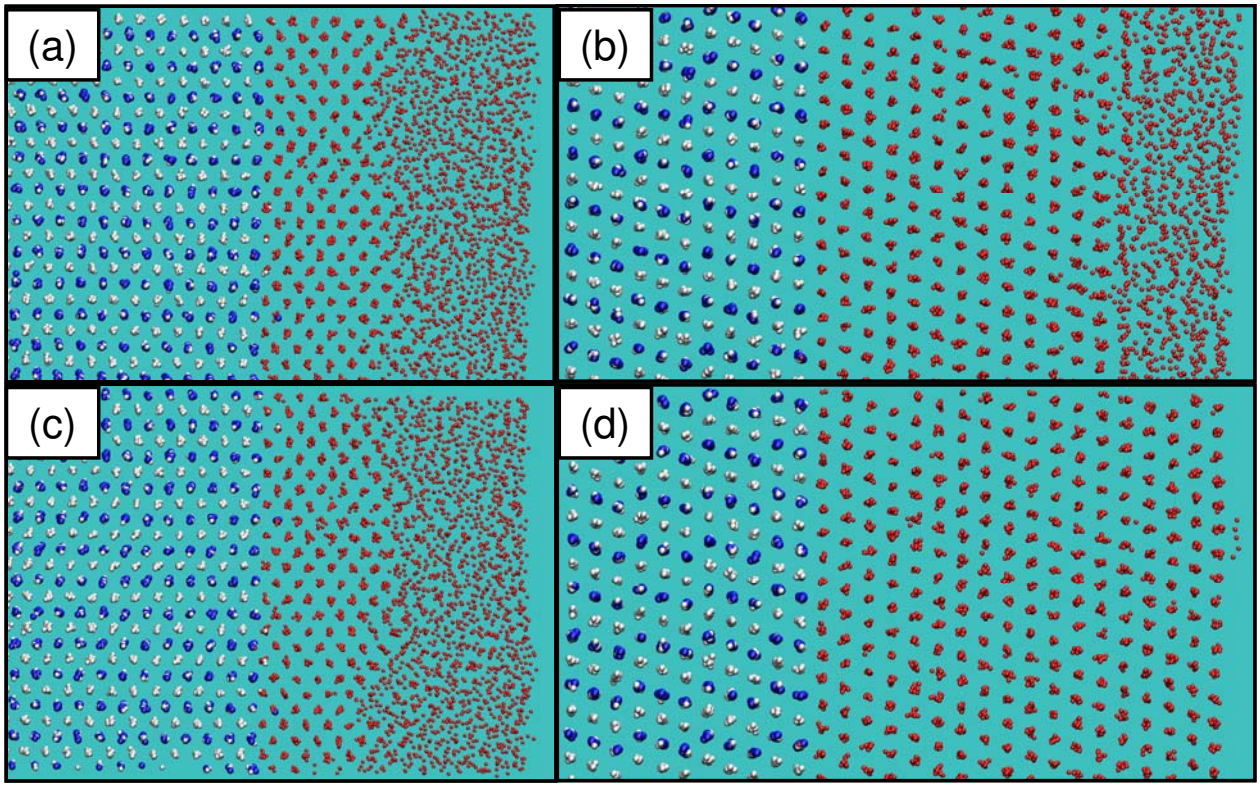

Fig. 3 The effect of anisotropic surfaces on the nucleation of solid Al from the melt at T = 860K. (a) t_s = 500ps, Al(110)//Al_3Ti(110) surface; (b) t_s = 500ps, Al(111)//Al_3Ti(112) surface; (c) t_s = 1200ps, Al(110)//Al_3Ti(110) surface; (d) t_s = 1200ps, Al(111)//Al_3Ti(112) surface.

because in our simulations there is only continuous one-dimensional growth with no fluctuations that transform embryos into critically sized nuclei. Future investigations focusing on extracting nucleation times will require the setting up a reliable threshold for differentiating nucleation and early stage of growth in one dimensional propagation, or creating a large system with enough liquid in order to embed a sufficiently large substrate into the bulk liquid and observe when each nucleus reaches its critical size.

We have considered two possible explanations for these observations: the anisotropy of the Al surface and interface energies (which is equivalent to the anisotropy of premelting temperatures reported previously [57, 58]); and the elastic energy associated with the lattice mismatch between solid Al and the substrate. As we now see, it is the interfacial free energies that determine the growth.

In Fig. 3, it is clearly seen that there is less solid in the outermost layer of the solid-liquid front on Al_3Ti(110) surface than that on Al_3Ti(112) surface. Although the solid-liquid interface for both surfaces are rough, similar to previous findings [59], the Al(111) S/L interface is relatively flat compared to that for Al(110) as can

be seen by comparing Fig. 3a to Fig. 3b, and Fig. 3c to Fig. 3d. The flatness of Al(111) S/L interface relative to the Al(110) interface suggests that the S/L interfacial energy is larger for Al(111) that for Al(110), as being flat minimizes the interfacial area, reducing this contribution to the energy. This means that the driving force to eliminate the (111) interface is greatest. One way to achieve this is to solidify all the liquid, but this means forming a new S/V interface. From Table 5 we see that the S/V surface energy for Al(111) is lowest, hence the energy penalty is smallest for this surface. Thus the net driving force for growth of the solid is greatest for the (111) surface. So we have one possible explanation for what we see.

The lattice mismatch for Al(110)//Al_3Ti(110) and Al(001)//Al_3Ti(001) is substantially greater than for Al(111)//Al_3Ti(112). The elastic energy associated with the lattice mismatch will thus be greater for Al(110)//Al_3Ti(110) and Al(001)//Al_3Ti(001) than for Al(111)//Al_3Ti(112), which will restrict any growth on the (110) and (001) surfaces. So we have a second possible explanation.

To help distinguish between these effects we repeated the simulations for the Al_3Ti(110)//Al(110) interface using twice the thickness of liquid. The solid formation again stopped before reaching the surface, with the liquid thickness being about the same as for the shorter cell. So this appears to suggest that it is not elastic energy that is restricting growth (we would then expect the thickness of solid to be the same for both cell lengths). However, there is a twist to the story. Increasing the liquid thickness increases the influence of the ordered Al on the lateral pressure of the cell, and hence of the relaxation of the cell perpendicular to the interface. It might therefore be that the Al stretches the substrate more when there is more Al in the cell, thereby obtaining a more favorable lattice constant for itself, making growth easier. However, we found very little difference in the interfacial dimensions following an increase in liquid thickness. This suggests that it is not the lattice mismatch that is dominating.

This raises the question: why is strain energy not playing a bigger part? We measured the lattice parameters for the Al_3Ti following the ordering of the Al. We found that the parameters *a* and *b* for the substrate had expanded to about 4.2Å, while *c* remained unchanged at 8.5Å. This results in a close lattice match between Al and Al_3Ti. It is not clear if this is a real phenomenon, or is instead an artifact of the potential, and requires further investigation.

Having established the reason for the observed ordering, we now examine its structure by considering the two dimensional structure factor $S_{2D}(k)$. This was calculated for four outer layers of interest, as indicated in Fig. 4a, and was averaged over 60 frames from 70 ps to 76 ps in each case. The wave vectors k_x and k_y were varied from $-100\times2\pi/L_x$ to $100\times2\pi/L_x$ and from $-100\times2\pi/L_y$ to $100\times2\pi/L_y$, respectively, where L_x and L_y are the dimensions of the computational cell in the plane of the interface. As we move further away from the Al_3Ti interface, fewer solid Al atoms are present as shown in Fig. 4a. This results in the hexagonal intensity pattern corresponding to a solid (111) interface decreasing gradually, as can be seen by comparing with Fig. 4e and Fig. 4d. However, the long range order still dominates in layer d because the pattern in Fig. 4d-II matches approximately to Fig. 4e-II. In layer c (Fig. 4c-I), we only have short range order, resulting in a hexagonal core surrounded by a liquid-like isotropic pattern in Fig. 4c-II. In layer b there are only small clusters of ordered phase, giving a very small ordered core surrounded by liquid-like isotropic pattern. Because it is closest to the melt, the positions of ordered atoms change randomly and the amount of ordering may also fluctuate in magnitude, resulting in the time-averaged short-ranged ordering being very weak in Fig. 4b-II. Therefore, clusters of ordered phase form and break down in a liquid-like environment.

C. Structural Ordering above the Al Melting Point

We now consider the ordering in the liquid Al near the Al_3Ti substrate above its melting point, and look for connections with the behavior of the liquid below the melting point that we have just discussed. Typical snapshots of ordering on the Al_3Ti (112) surface are shown in Fig. 5 for temperatures 165K (a) and 15K (b) above the melting point. To characterize the ordering of atoms into planes parallel to the interface, we have computed one dimensional density profiles $\rho(z)$, where z is the distance along the axis perpendicular to the interface. Each profile was obtained as an average over a period of 5 ps spanning the last 5000 steps after a 300 ps NPT run. The density profile is strongly periodic in the Al_3Ti crystal, being centered tightly on the lattice positions for both the Ti atom density (blue) and Al atom density (red). At the S/L interface, the oscillations dampen gradually until the uniform density of the liquid phase is reached. In this region, not only the initial liquid atoms appear in the ordered layers (green in Fig. 5a,b) but also dissolved Al and Ti atoms, as shown in Fig. 5a. The density profile at a higher temperature decays faster as a function of the distance from the interface than the density profile at a low temperature. At a temperature just above the melting

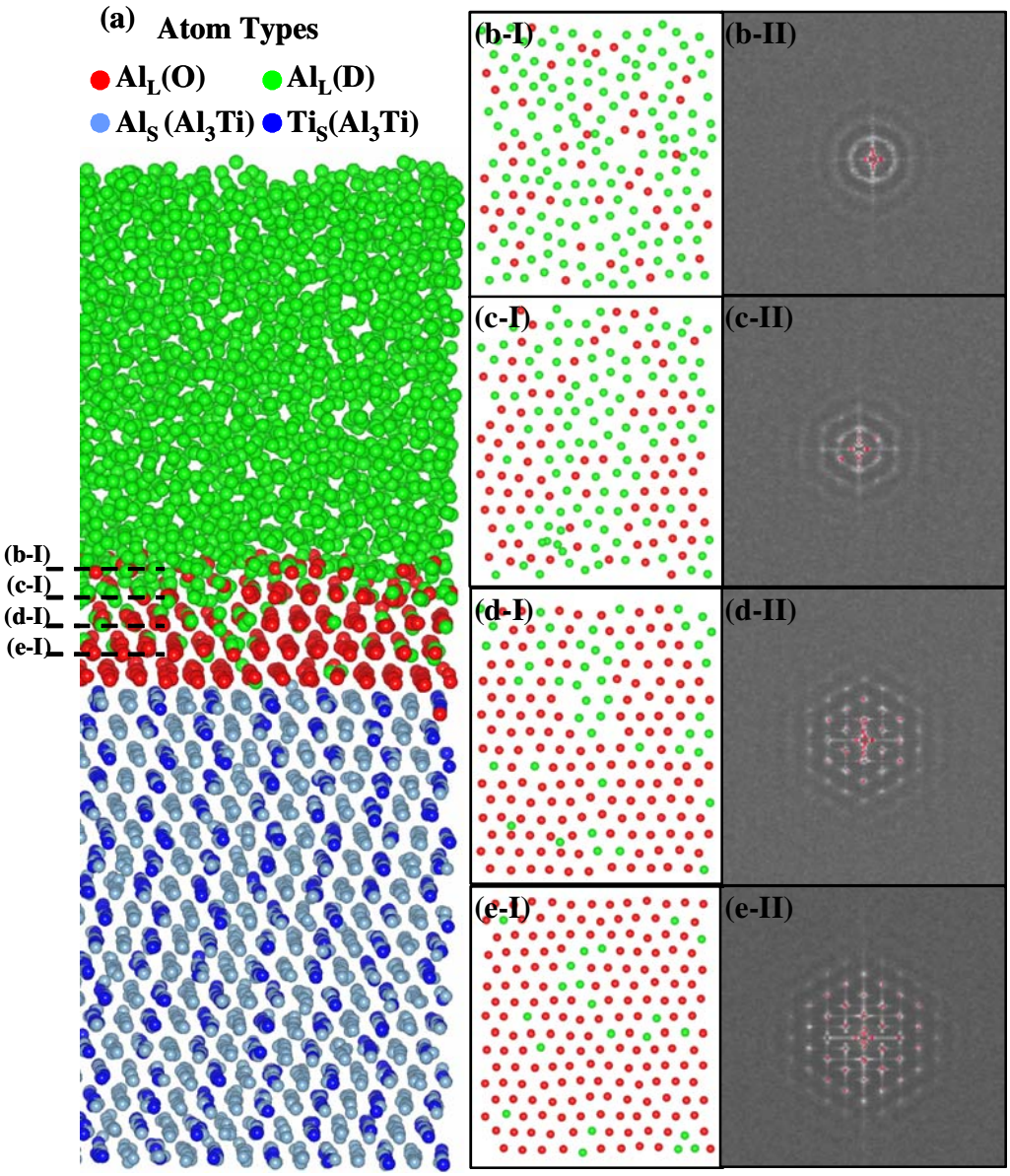

Fig. 4 Structural ordering at the beginning of continuous growth on Al_3Ti (112) surface at 860K. (a) a snapshot at t_s = 70ps, and projections of the outer four layers (b-e I) and the corresponding time-averaged structure factors for 6ps (b-e II). Ti and Al atoms in Al_3Ti structure are in blue and light blue, respectively. Ordered solid-like Al (O) are in red and disordered liquid Al (D) are in green.

point (T = 875 K), strong ordering of Al atoms is seen close to the Al_3Ti surface and it extends 9 layers into the liquid. We note that once solid-like layers form on an Al_3Ti substrate with a size on the scale of micrometers, liquid atoms are in direct contact with their own solid phase, and so no nucleation barrier need be overcome upon freezing.

Since different surfaces have different nucleation potentials, we now analyze any variation in liquid ordering with surface to see if there is any correlation. To characterize the ordering thickness and decay mode we need a quantitative measure of the density profile. Here we consider three possibilities: a phase field variable, a disorder parameter, and interplanar spacing.

In phase field theory, the variable ϕ can be regarded as the envelope of the density profile [60]. For a pure system, the one dimensional (planar interface) solution of the phase field model gives [60]:

$$\phi(z) = \frac{1}{2}\left[1 + \tanh\left(\frac{z}{2\delta_A}\right)\right] \tag{6}$$

where ϕ varies in the z direction normal to the interface, and δ_A is a measure of interface thickness. We have computed the phase field variable from the density profile using:

$$\phi(z) = \frac{\rho_{peak}^{(z)} - \overline{\rho}_{liquid}}{\rho_{\max} - \overline{\rho}_{liquid}} \tag{7}$$

where $\rho^{(z)}_{peak}$ is the peak height of the density, $\overline{\rho}_{liquid}$ is average density in the liquid, and ρ_{max} is the largest peak height in the solid-like layers closest to the solid Al_3Ti substrate. The density profile is thus normalized to give a smooth transition from liquid ($\phi = 0$) to solid ($\phi = 1$). Using Eq.6, we can compute the quantity z/δ_A from the phase field variable

$$z/\delta_A = 2\,\mathrm{arctanh}\,(2\phi - 1) = g(\phi) \tag{8}$$

as shown in Fig. 5c. The confidence computed for the density profiles fitted to Eq.6 on different surfaces of Al_3Ti only reaches 75%, which is quite poor. The error is particularly significant close to the bulk solid or bulk liquid. This indicates that the analytical solution assuming equilibrium at the melting temperature may not be a good choice to quantify the ordering above the melting point (T = 875 K).

Another function developed from mean field theory was initially proposed by Tarazona and Vicente [61] to study oscillating forces in liquids acting on walls and characterize the constructive/destructive interference between the local ordering induced by the boundaries. This was reformulated separately by Hashibon *et al.* [18]

and Tomagnini *et al.* [62]. According to them, the density profile of ordering layers on a solid substrate above the melting temperature can be effectively characterized by an exponential decay function:

$$\rho(z) = C_0 e^{-\kappa z} + \rho_l \tag{9}$$

where κ is the disorder parameter, z is the distance from the substrate, C_0 is a constant, and ρ_l is a fitting parameter to account for the background liquid density. This decay function is an envelope of the density profile as plotted against distance from the $Al_3Ti(112)$ surface in Fig. 5a. Therefore, the following function is linear as a function of distance from the Al_3Ti surfaces:

$$f[\rho(z)] = \ln[(\rho(z) - \rho_l)] = -\kappa z + \varepsilon \tag{10}$$

where ε is a constant. As shown in Fig. 5c, the fitted lines and the measured points are closely related on three orientations of Al crystal at 875K. Small divergences between the fitted and the measured values are

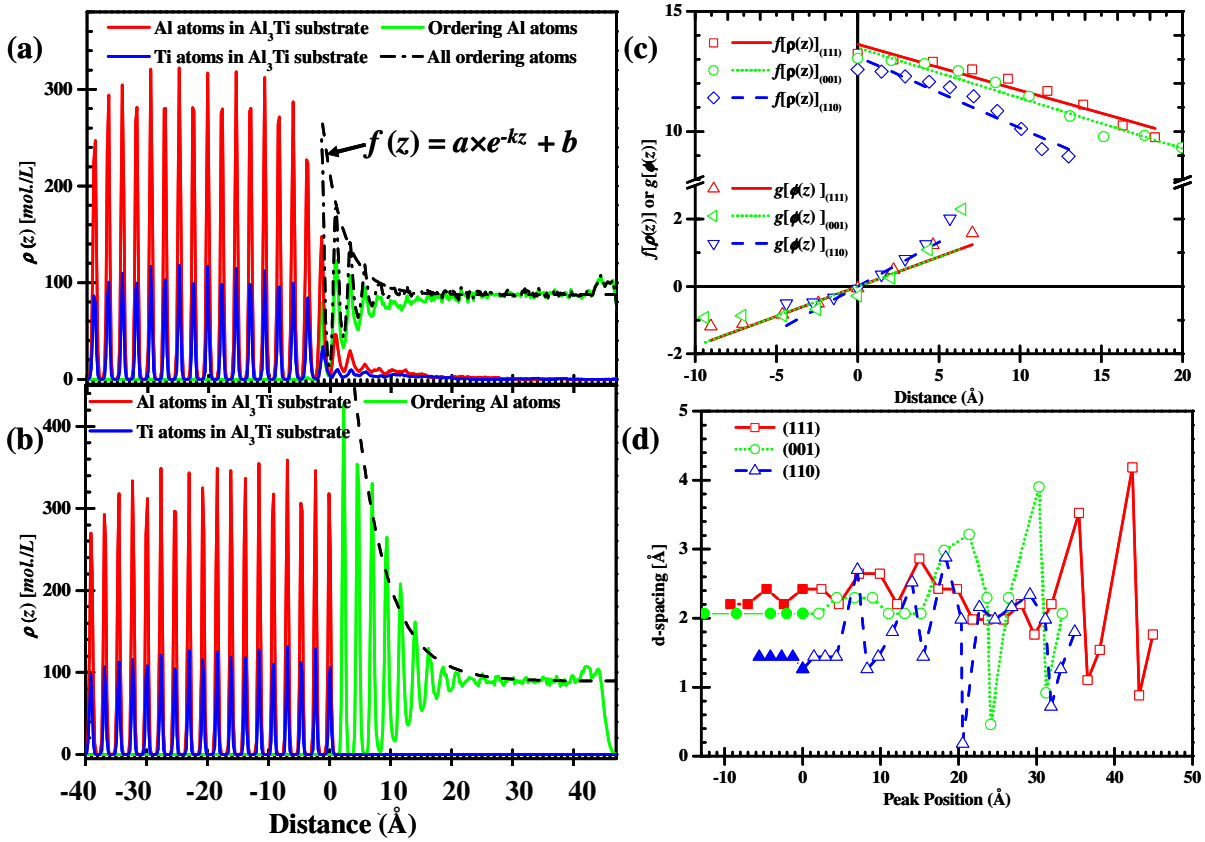

Fig. 5 Structural ordering on $Al_3Ti(112)$ surface at high temperatures: (a) T = 1025K; (b) T = 875K; (c) the density profiles for different orientations at T = 875 K fitted to two different functions($f[\rho(z)]$ and $g[\phi(z)]$), (d) layer separation across the samples at T =1000 K. The filled symbols are within the Al_3Ti substrate, and the open symbols are within the liquid.

seen on the (110) surface because the roughness of this interface is high. The disorder parameter is given by the fitted line's slope.

The distance between density peaks can also give a measure of d-spacing (the interlayer distance) for a particular orientation. Local peaks corresponding to the maxima in the density profile were identified by searching in consecutive bins. Fig. 5d shows the distance between consecutive peaks on three different interface directions at 1000 K. The filled symbols are the d-spacing in solid Al_3Ti which is followed by the quasi-solid region within the liquid and then the complete liquid where the ''maxima'' are in random locations instead of periodic. The solid-like layers extend 9~18 Å into the liquid and they expand gradually before ordering terminates, especially on the (111) and (001) surfaces where the d-spacing is large.

In order to analyze the decay of the density profile as a function of temperature and substrate orientation, the envelope of the density profile was extracted and fitted to Eq. 9. As shown in Fig. 6. three orientations (111), (001) and (110), at temperatures ranging from 875K to 1025K in 25K steps, were studied and the corresponding disorder parameter plotted. Because of the presence of the Al_3Ti/liquid interface, significant dissolution of Al_3Ti into the liquid was observed above 1025K, which makes reliable fitting of a density profile to an exponential function in such narrow ordering layers very difficult (there are one or two peaks at most and the fitting is no longer accurate). We also found that the reliability of the disorder parameter depends on the number of layers in the substrate, similar to a previous study [18]. Stable results were achieved when the substrate was composed of more than 10 layers of atoms. As can be seen in Fig.6, the amount of disorder is very similar for the (111) and (001) surfaces, and they are both smaller than for the (110) surface, agreeing well with previous work [18]. This agreement with the work of Hashibon et al [18] is particularly interesting because of the different methodologies used for the simulations: we do not fix the atoms in the substrate and some of them diffuse into the liquid. We note that the large variation in the disorder parameter data for the (110) surface (including a change in slope in its temperature dependence) shown in Fig.6 may be a consequence of the difficulty in generating density profiles from such a rough surface, even though a time average was used. We believe the solid-like layers extend further into the liquid on the Al_3Ti(112) and (001)

surfaces than when placed on Al_3Ti (110), as shown in Figs. 5c, and d, because Al_3Ti(112) and (001) surfaces are close-packed and so can bond Al atoms more tightly than the more open (110) plane.

According to previous studies [18, 62], the disorder parameter is inversely proportional to the d-spacing. However, it is not true if the expansion of lattice parameter in the substrate upon temperature increase is taken into account. As shown in Fig.6, the d-spacing decreases as temperature is reduced, indicating that the relationship between k and d-spacing may not be linear. However, it does give a good estimation of the disorder parameter on the three different interfaces. For example, the (111) surface has the largest d-spacing and the disorder parameter tends to be the smallest.

If we now try to correlate the ordering in the liquid above the melting point with the growth seen just below, we find that the Al_3Ti(112)//Al(111) is favored in both cases, and Al_3Ti(110)//Al(110) fares poorly in both cases. So this looks promising. The Al_3Ti(001)//Al(001) system is less clear, however. So, can we use the faster high temperature simulations to identify good nucleants? Our small set of results suggests that the clear cases can be discriminated, but promising candidates will need further investigation with lower temperature simulations.

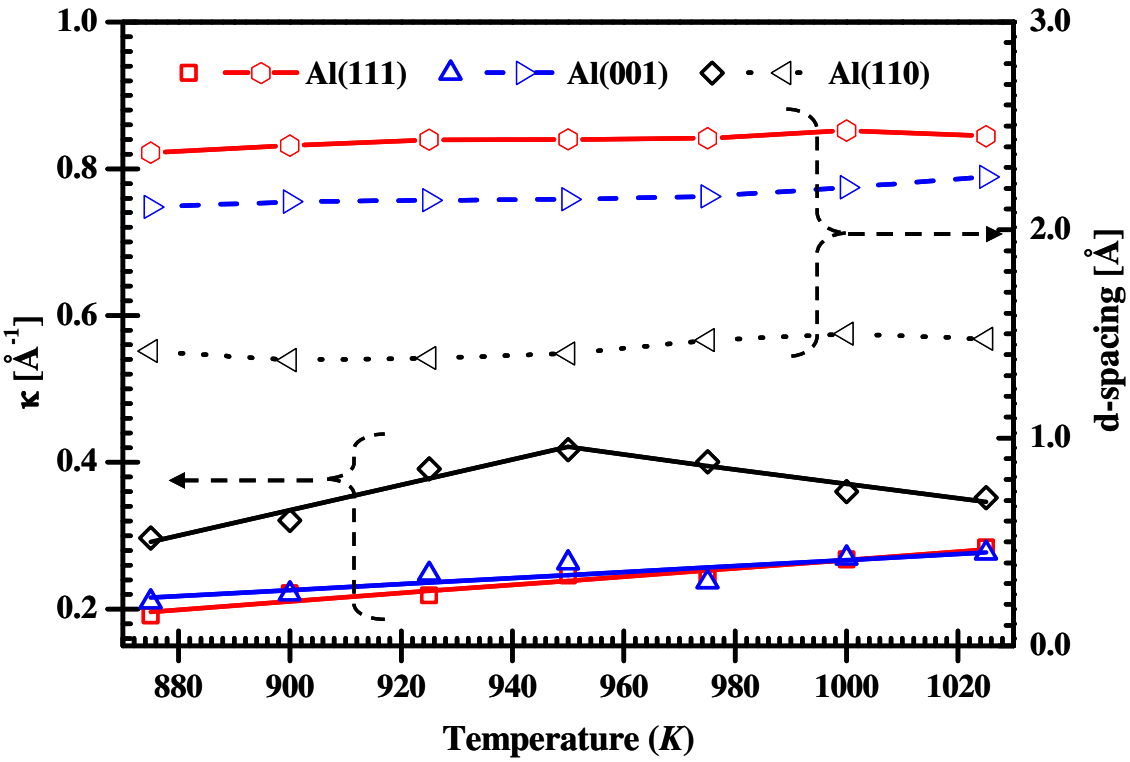

Fig. 6 The d-spacing (top three lines) and disorder parameter *k* (bottom three lines) as a function of temperature.

IV. SUMMARY AND CONCLUSIONS

By means of molecular dynamics simulations, we have investigated structural ordering above the melting point of Al and heterogeneous nucleation of α-Al from the Al melt upon cooling. To accomplish this we first modified the EAM potential of Zope and Mishin [24] to predict correctly the stable structure of Al_3Ti, using data generated from *ab initio* MD. Using the new Al-Ti EAM potentials, we performed classical molecular dynamic simulations to observe the initial stage of solidification in Al melts at small undercoolings. We find that complete growth of α-Al occurs only on the (112) face of Al_3Ti, showing that this is a preferred substrate. We believe this is due to anisotropy in the S/L and S/V interfacial energies: growth is promoted by high S/L and low S/V interfacial energies. In our simulations, elastic strain appears not to play a part, but this is because of a relaxation (possibly unphysical) of the substrate to release the strain due to mismatch. Thus, the Al_3Ti(112) substrate effectively initiates free growth when a small driving force (local undercooling) is given, explaining the orientation relationships at the Al/Al_3Ti interface reported previously from experiments [5, 17, 63, 64].

Structural ordering was clearly seen in the liquid close to the Al_3Ti substrate at temperatures above the Al melting point. The disorder parameter decays as temperature decreases, agreeing well with previous findings [18]. Interestingly, the disorder parameter is not a simple function of d-spacing, as suggested by previous studies using rigid substrate [18], though there is a clear correlation. The dependence of the degree of ordering with substrate surface corresponds well to the ease of solid growth at low undercooling. This suggests that simulations above the melting point can be used to identify potential good nucleant materials.

ACKNOWLEDGEMENTS

The authors would like to acknowledge funding from King Abdullah University of Science and Technology (KAUST), and support from Thomas Young Centre (TYC) at Imperial College London. The authors also acknowledge many useful discussions both with colleagues at Imperial College London, Oak Ridge National Laboratory, and Ford Research and Advanced Engineering Lab. and, especially Stefano Angioletti-Uberti, Professors Mike Finnis, James R. Morris, and Drs. Mei Li and John Allison.

REFERENCES

1 W. Rosenhain, J. D. Grogan, and T. H. Schofield, Jour. Inst. Metals **44**, 305 (1930).

2 B. Murty, S. Kori, and M. Chakraborty, Int. Mater. Rev. **47**, 3 (2002).

3 L. Arnberg, L. Backerud, and H. Klang, in *Grain refinment in castings and welds*, edited by G. J. Abbaschian and S. A. David (AIME, Warrendale, PA, 1983).

4 L. Arnberg, L. Backerud, and H. Klang, Met. Techn. **9**, 1 (1982).

5 P. Schumacher, A. L. Greer, J. Worth, P. V. Evans, M. A. Kearns, P. Fisher, and A. H. Green, Mater. Sci. Techn. **14**, 394 (1998).

6 P. Schumacher and A. L. Greer, in *Light Metals*, edited by W. Hale (TMS, Anaheim, USA, 1996), p. 745.

7 P. Schumacher and B. J. McKay, Journal of Non-Crystalline Solids **317**, 123 (2003).

8 N. Iqbal, N. H. van Dijk, S. E. Offerman, M. P. Moret, L. Katgerman, and G. J. Kearley, Acta Mater. **53**, 2875 (2005).

9 N. Iqbal, N. H. van Dijk, S. E. Offerman, N. Geerlofs, M. P. Moret, L. Katgerman, and G. J. Kearley, Mater. Sci. Eng. A **416**, 18 (2006).

10 N. Iqbal, N. H. van Dijk, S. E. Offerman, M. P. Moret, L. Katgerman, and G. J. Kearley, Journal of Non-Crystalline Solids **353**, 3640 (2007).

11 M. Easton and D. St.John, Metall. Mater. Trans. A **30A**, 1613 (1999).

12 M. Easton and D. St.John, Metall. Mater. Trans. A **30A**, 1625 (1999).

13 M. X. Zhang, P. M. Kelly, M. A. Easton, and J. A. Taylor, Acta Mater. **53**, 1427 (2005).

[14] M. X. Zhang, S. Q. Chen, H. P. Ren, and P. M. Kelly, Metall. Mater. Trans. A **39**, 1077 (2008).

[15] M. S. Daw and M. I. Baskes, Phys. Rev. Lett. **50**, 1285 (1983).

[16] M. Daw and M. Baskes, Physical review. B, Condensed matter and materials physics **29**, 6443 (1984).

[17] A. L. Greer, A. M. Bunn, A. Tronche, P. V. Evans, and D. J. Bristow, Acta Mater. **48**, 2823 (2000).

[18] A. Hashibon, J. Adler, M. W. Finnis, and W. D. Kaplan, Comp. Mater. Sci. **24**, 443 (2002).

[19] M. S. Daw and M. I. Baskes, Physical Review B **29**, 6443 (1984).

[20] M. Daw, S. Foiles, and M. Baskes, Materials science reports **9**, 251 (1993).

[21] M. W. Finnis and J. E. Sinclair, Philos. Mag. A **50**, 45 (1984).

[22] F. Ercolessi, M. Parrinello, and E. Tosatti, Philos. Mag. A **58**, 213 (1988).

[23] D. Farkas, Modell. Sim. Mater. Sci. Eng. **2**, 975 (1994).

[24] R. R. Zope and Y. Mishin, Physical Review B **68**, 024102 (2003).

[25] C. Colinet and A. Pasturel, Intermetallics **10**, 751 (2002).

[26] W. Smith and T. R. Forester, Journal of Molecular Graphics **14**, 136 (1996).

[27] I. T. Todorov, W. Smith, and T. R. Forester, STFC Daresbury Laboratory, UK, 2009).

[28] S. J. Plimpton, J Comp Phys **117**, 1 (1995).

[29] S. Plimpton, P. Crozier, and A. Thompson, Sandia National Laboratories, Albuquerque, NM, USA, 2009).

[30] M. P. Allen and D. J. Tildesley, *Computer Simulation of Liquids* (Clarendon Press. , Oxford, 1989).

[31] P. Norby and A. Norlund Christensen, Acta Chemica Scandinavica A **40**, 157 (1986).

[32] W. G. Hoover, Physical Review A **31**, 1695 (1985).

[33] D. Buta, M. Asta, and J. J. Hoyt, Phys. Rev. E **78**, 031605 (2008).

[34] J. D. Honeycutt and H. C. Andersen, The Journal of Physical Chemistry **91**, 4950 (1987).

[35] C. L. Kelchner, S. J. Plimpton, and J. C. Hamilton, Physical Review B **58**, 11085 (1998).

[36] H. Tsuzuki, P. S. Branicio, and J. P. Rino, Computer Physics Communications **177**, 518 (2007).

[37] J. Morris and X. Song, The Journal of chemical physics **119**, 3920 (2003).

[38] M. P. Allen and D. J. Tildesley, *Computer Simulation of Liquids* (Oxford University Press, Oxford, 1987).

[39] F. Ercolessi and J. B. Adams, Europhysics Letters **26**, 583 (1994).

[40] G. Kresse and J. Hafner, Phys. Rev. B **47**, 558 (1993).

[41] G. Kresse and J. Hafner, Phys. Rev. B **49**, 14251 (1994).

[42] G. Kresse and J. Furthmüller, Comput. Mat. Sci. **6**, 15 (1996).

[43] G. Kresse and J. Furthmüller, Phys. Rev. B **54**, 11169 (1996).

[44] G. Kresse and J. Joubert, Phys. Rev. B **59** (1999).

[45] P. E. Blöchl, Phys. Rev. B **50** (1994).

[46] J. P. Perdew, J. A. Chevary, S. H. Vosko, K. A. Jackson, M. R. Pederson, D. J. Singh, and C. Fiolhais, Phys. Rev. B **46**, 6671 (1992).

[47] J. P. Perdew, J. A. Chevary, S. H. Vosko, K. A. Jackson, M. R. Pederson, D. J. Singh, and C. Fiolhais, Phys. Rev. B **48**, 4978 (1993).

[48] P. Brommer and F. Gähler, Modelling Simul. Mater. Sci. Eng. **15**, 295 (2007).

[49] G. Ghosh and M. Asta, Acta Mater. **53**, 3225 (2005).

[50] F. R. de Boer, R. Boom, W. C. M. Mattens, A. R. Moedema, and A. H. Niessen, *Cohesion in Metals* (North-Holland, Amsterdam, 1988).

[51] W. R. Tyson and W. A. Miller, Surf Sci. **62**, 267 (1977).

[52] C. I. Smithels, *Metals Reference Book* (Butterworths, London, 1976).

[53] J. Schuster and M. Palm, Journal of phase equilibria and diffusion **27**, 255 (2006).

[54] J. R. Morris, C. Z. Wang, K. M. Ho, and C. T. Chan, Physical Review B (Condensed Matter) **49**, 3109 (1994).

[55] J. R. Morris and X. Song, The Journal of Chemical Physics **116**, 9352 (2002).

[56] R. S. Aga, J. R. Morris, J. J. Hoyt, and M. Mendelev, Phys. Rev. Lett. **96**, 245701 (2006).

[57] J. J. Hoyt, D. Olmsted, S. Jindal, M. Asta, and A. Karma, Phys. Rev. E **79**, 020601 (2009).

[58] H. Song, S. J. Fensin, M. Asta, and J. J. Hoyt, Scripta Mater. **63**, 128 (2010).

[59] J. R. Morris, M. I. Mendelev, and D. J. Srolovitz, Journal of Non-Crystalline Solids **353**, 3565 (2007).

[60] W. J. Boettinger, J. A. Warren, C. Beckermann, and A. Karma, Ann. Rev. Mater. Res. **32**, 163 (2002).

[61] P. Tarazona and L. Vicente, (Taylor & Francis, 1985), Vol. 56, p. 557

[62] O. Tomagnini, F. Ercolessi, S. Iarlori, F. D. Di Tolla, and E. Tosatti, Phys. Rev. Lett. **76**, 1118 (1996).

[63] I. Maxwell and A. Hellawell, Acta Metall. **23**, 229 (1975).

[64] M. Easton, Metall. Mater.Trans. A **36A**, 1911 (2005).